Fractography combined with unsupervised pattern recognition of acoustic emission signals for a better understanding of crack propagation in adhesively bonded wood

Gaspard Clerc[1,4] · Markus G. R. Sause[2] · Andreas J. Brunner[3] · Peter Niemz[1] · Jan-Willem G. van de Kuilen[4,5]

Abstract

In this paper, acoustic emission (AE) signals obtained during quasi-static crack propagation in adhesively bonded beech wood were classified using an unsupervised pattern recognition method. Two ductile one-component polyurethane (1C-PUR) adhesives with the same formulation except for one system being reinforced with short polyamide (~ 1 mm long) fibers were compared to a relative brittle phenol–resorcinol–formaldehyde (PRF) adhesive. Using only localized AE signals, it was shown that the signals originating from the crack propagation could be classified into two different clusters. Comparing the AE signals with a new fractography method, it was estimated that different clusters are due to distinct failure mechanisms, with signals of cluster 1 being associated with wood failure and signals of cluster 2 with adhesive failure. The obtained results suggest that for the PRF adhesive the wood fibers help to slow down the crack propagation. A similar but lesser effect was noted for the polyamide fibers added to the 1C-PUR adhesive matrix.

Gaspard Clerc
gaspard.clerc@bfh.ch

[1] Architecture, Wood and Civil Engineering, BFH, Bern University of Applied Sciences, Solothurnstrasse 102, 2500 Biel, Switzerland

[2] Institute of Materials Resource Management, University of Augsburg, Universitätstrasse 1, 86159 Augsburg, Germany

[3] Laboratory for Mechanical Systems Engineering, Empa, Swiss Federal Laboratories for Materials Science and Technology, Überlandstrasse 129, 8600 Dübendorf, Switzerland

[4] Wood Technology, Technical University of Munich, Winzererstrasse 45, 80797 Munich, Germany

[5] TU Delft, Faculty of Civil Engineering and Geosciences, Biobased Structures and Materials, Stevinweg 1, 2628 Delft, The Netherlands

Introduction

The current development of adhesives for timber load-bearing structures must meet the performance requirements and at the same time reduce the ecological and health impact of the adhesives used. Thus, the adhesive industry is trying to develop new adhesives as an alternative to the PRF adhesive system, which have, despite their high mechanical performance, the disadvantage of containing a significant proportion of formaldehyde, a substance known to be cancerogenic. One of the best currently available alternatives to these systems are 1C-PUR systems, but despite encouraging results (Lehringer and Gabriel 2014), the performance of 1C-PUR adhesives is still below that of long-used commercial systems such as the PRF. The exact reason explaining why the PRF system is generally performing better in terms of strength and delamination resistance is still not completely understood. One possible explanation could originate from the fracture behavior. Generally, a rupture of the bond line in the wood layer is preferable (and recommended by the EN 14080 standard, for example) as it implies that the adhesive is stronger than the wood. However, it was shown that the proportion of the fracture surface occurring in the wood layer, i.e., the wood fracture percentage (WFP), does not correlate with the strength of the bond line and that depending on the wood origin, strong variations can be observed (Hass et al. 2014). Typically, lap shear samples of adhesively bonded wood show no strength differences between 1C-PUR and PRF (in dry climate), but PRF-bonded samples generally have a higher WFP than 1C-PUR-bonded samples (Kläusler et al. 2014). Clerc et al. (2019) have shown that under cyclic loading, crack propagation under Mode II 4-ENF is slower and demands higher energy for PRF samples than for 1C-PUR samples despite showing a relatively similar energy release rate (ERR) under quasi-static loading. Here, too, 1C-PUR adhesives typically show a failure at the interface between the wood and the adhesive, whereas PRF generally shows a higher wood fracture percentage. The question is, therefore, whether the better performance of PRF adhesive can be partly explained by the failure layer located in the wood, where its fibrous nature helps to reduce the crack propagation speed compared to a propagation in the adhesive interface. Typically, a crack stopped by a fiber during its propagation will branch (supposing that the fracture toughness of the crack propagation domain is lower than that of the fibers) to overcome the obstacle. Due to the branching of the crack, more surface is created, and an on average smaller damage size can be expected. It is, however, difficult to know whether the wood fibrous structure is really reducing the rate of crack propagation as the observation of the fracture surface is only possible a posteriori.

The use of AE to monitor damage accumulation in wood material in situ (Aicher et al. 2001; Jakieła et al. 2008; Reiterer et al. 2000) is a suitable method to complement common mechanical tests as it permits the detection of the associated accumulation and interaction of damage in the full specimen volume with sub-microsecond time resolution. One difficulty of the AE method is the identification of the AE signal origin, with respect to both the microscopic source mechanism and its exact location and orientation. Concerning this issue, fractography

combined with AE-based parameter analysis has been used to identify microscopic failure mechanism in wood (Ando et al. 2006) and in bamboo (Chen et al. 2018). Unsupervised pattern recognition (UPR) methods based on AE frequency and/or AE time domain features have been successfully used to characterize wood failure (Baensch et al. 2015a; Diakhate et al. 2017; Najafi et al. 2017). These methods seek the numerically best partition of signals according to selected features into different clusters to possibly identify different natural classes of AE signals (Sause et al. 2012a). To associate these natural classes with physical features, a detailed analysis of the fracture surface/volume should be conducted using for example multiphysics finite element method (Sause et al. 2012b), nondestructive testing (Baensch et al. 2015b) or fractography. In wood under tensile stress, Baensch et al. 2015b could combine AE with in situ synchrotron X-ray micro-computed tomography to determine the main failure mechanisms were interwall cracks (cell wall debonding) and cell wall cracks. However, the use of UPR and X-ray CT on plywood miniature specimens yielded the same two AE clusters as obtained for clear wood (Brunner et al. 2015); no separate AE cluster could be assigned solely to the adhesive. One possible explanation could be that for the chosen sample geometry (dog-bone tensile sample), the maximal stresses generally do not occur in the bond line but rather in the wood. In this paper, AE was used to monitor the damage accumulation of adhesively bonded wood under quasi-static Mode II 4-ENF loading. Using this test setup, the maximal shear stresses are occurring in the bond line of the sample. The AE signals were recorded from three wood adhesives (two relatively ductile 1C-PURs and one relatively brittle PRF system). This setting was chosen to better understand how the structure of the wood adhesive compound influences the crack propagation and how damages evolve for each adhesive system. For this reason, small polyamide fibers were added to the matrix of one of the 1C-PUR adhesives, being otherwise identical. AE signals obtained during the test were then analyzed with an unsupervised pattern recognition to identify natural clusters. A new fractography method is presented to potentially explain the microscopic origin of these different clusters.

Materials and methods

Experimental setup

Mechanical test setup

Beech wood (*Fagus sylvatica* L.) with a mean density of 714 kg/m^3 at a wood moisture content of 12% was used for the tests. The wood had no defects such as knots or grain deviation. Prior to the adhesive bonding, a 15-µm-thick fluoropolymer (ETFE230N) foil was applied between the lamellae on the first 120 mm to simulate a starter crack. Three adhesives are compared in the tests: The first is a relatively brittle phenol–resorcinol–formaldehyde (PRF, trade name (Aerodux 185) and two are ductile one-component polyurethane (1C-PUR) adhesives with a low modulus of elasticity (MOE). These two 1C-PUR adhesives are based on the same

polymer, with the difference that additional small polyamide fibers (~1 mm length and ~0.1 mm diameter) were introduced into the adhesive matrix of the LOCTITE HB 110 PURBOND (short name HB 110), but not into the LOCTITE VN 3158 (short name: VN 3158). Once cured, the front position of the foil was referenced as position of the crack tip, and the pre-crack length was set to 110 mm. The samples were then cut to a width of 20 mm, a crack length of 110 mm and a length of 317 mm. The adhesively bonded wood joints were stored for several days at 23 °C and 50% relative humidity prior to testing. The end-notched flexure (ENF) specimens were loaded under quasi-static displacement control at 1 mm/min in 4-point bending Mode II. The test was performed on a servo-hydraulic test machine (type 1237 Instron) equipped with a 1 kN load cell with a load and displacement accuracy of at least 1% of the measured value.

AE test setup

AE equipment (type AMSY-6) and preamplifier (type AEP-3 with a hardware bandpass between 30 and 1000 kHz from Vallen Systeme GmbH) with 150 kHz resonant sensors (type SE-150 M from Dunegan Engineering Corp.) and one broadband sensor (type S9208 from Physical Acoustics Corp.) were used. Data acquisition settings were: acquisition threshold 40 dB_{AE}, duration discrimination time 400 µs and a rearm time of 1 ms. Two SE-150 M AE sensors were placed on top and bottom each between the bottom and top loading rollers, and between the top loading rollers, respectively. In addition, one S9208 sensor was placed on the bottom side between the top loading rollers (see Fig. 1 for details). All sensors were coupled with a silicone-free vacuum grease and mounted with metal springs.

For assessing the delamination length as a function of time, linear AE signal source location was performed with the four sensors mounted on the bottom side of the joint. The signal sources were localized using two different 1-D localization processors to find signals, which were correctly identified by the four sensors 2–7–4–6 (see Fig. 1). Using this method, only AE wave propagation in the longitudinal direction was considered, meaning that only one speed of propagation ($v = 4250$ m/s) could be used. The AE source location accuracy was checked via the so-called

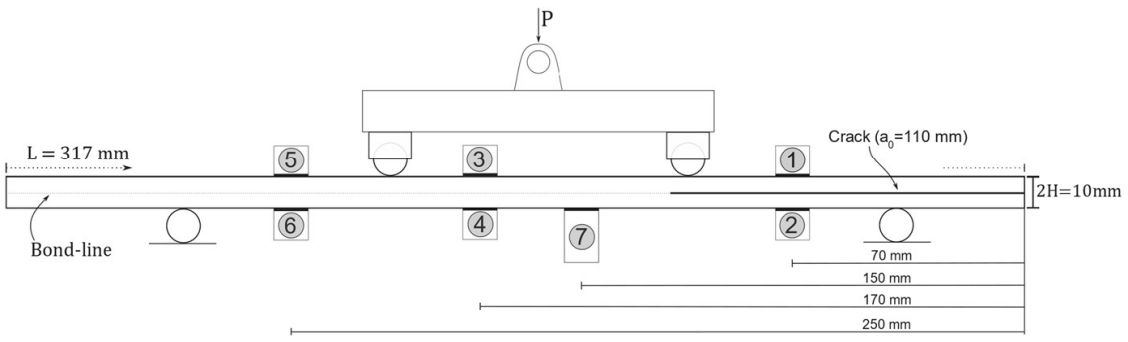

Fig. 1 Scaled schematic representation of the test setup, with the type and position of each AE sensor—the type of sensor for sensors 1–6 is SE-150M and S9208 for the sensor 7

autocalibration for which each sensor in turn was used as emitter of elastic waves, which were recorded by the other sensors and localized.

Unsupervised pattern recognition (UPR) methodology

The UPR used in this work was adapted from earlier researches on composites (Sause et al. 2012a) and has been previously applied to wood failure (Baensch et al. 2015a). The algorithm is based on an exhaustive search procedure of AE features and identifies the most suitable partition without initial assumptions regarding the number of AE features used and the number of clusters. To this end, a list of $K=9$ frequency-based AE features were defined to use for the investigation (see Table 1). The selection of the number of partial powers (6 in this case) in the AE feature set, in principle, is arbitrary, but experience has shown that 6 is a reasonable choice in terms of computational effort and results (Sause et al. 2012a; Sause and Horn 2013). Boundary constraints for the algorithm were chosen as $M=3$ minimum number of features to use for a partition and $P=10$ as maximum number of clusters expected. Based on these boundary constraints, the algorithm investigates all $\binom{M}{K} \cdot (P-1)$ partitions and ranks the obtained result using cluster validity metrics (Sause et al. 2012a). For this investigation, Gaussian mixture models were chosen as clustering algorithm with normalization of features using their unit variance.

Fractography

It is hypothesized that different AE signal clusters revealed by UPR are representing different fracture layers in or near the bond line. The distinction between the different fracture layers on the fracture surface is relatively easy for PRF adhesive as

Table 1 AE features used for the investigation

Peak frequency	f_{peak}	[Hz]
Frequency centroid	$f_{\mathrm{centroid}} = \frac{\int f \cdot \tilde{U}(f)\mathrm{d}f}{\int \tilde{U}(f)\mathrm{d}f}$	[Hz]
Weighted peak frequency	$f_{\mathrm{peak}} = \sqrt{f_{\mathrm{peak}} \cdot f_{\mathrm{centroid}}}$	[Hz]
Partial power	$\int_{f_1}^{f_2} \tilde{U}^2(f)\mathrm{d}f \,/\, \int_{f_{\mathrm{start}}}^{f_{\mathrm{end}}} \tilde{U}^2(f)\mathrm{d}f$	[%]
	$f_{\mathrm{start}} = 0$ kHz	
	$f_{\mathrm{end}} = 1200$ kHz	
	Partial power 1: $f_1 = 0$ kHz; $f_2 = 150$ kHz	
	Partial power 2: $f_1 = 150$ kHz; $f_2 = 300$ kHz	
	Partial power 3: $f_1 = 300$ kHz; $f_2 = 450$ kHz	
	Partial power 4: $f_1 = 450$ kHz; $f_2 = 600$ kHz	
	Partial power 5: $f_1 = 600$ kHz; $f_2 = 900$ kHz	
	Partial power 6: $f_1 = 900$ kHz; $f_2 = 1200$ kHz	

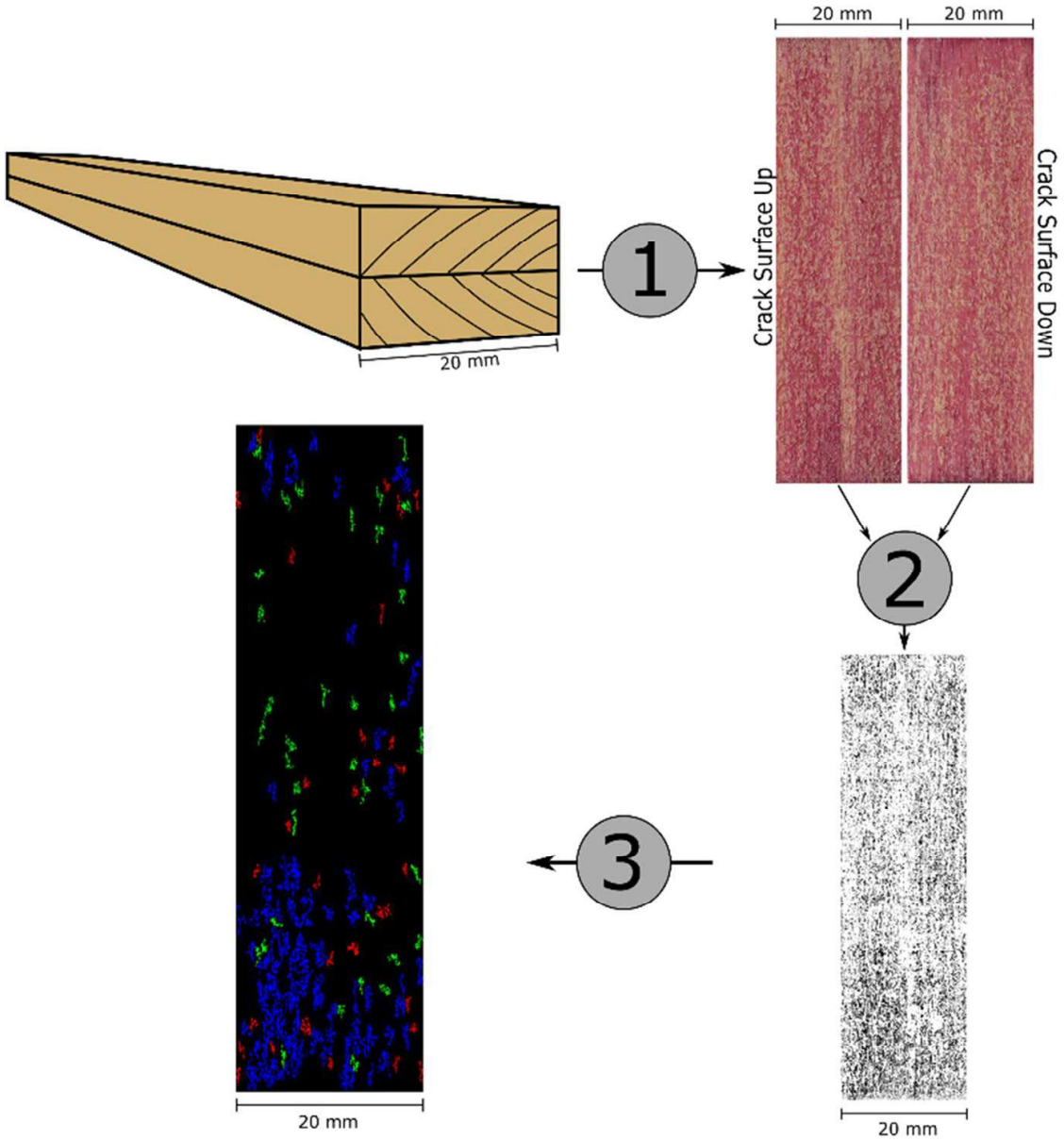

Fig. 2 Schematic of the main steps of the fractography analysis method—see text for a detailed description of the method

the contrast between the wood and the adhesives' dark color allows distinguishing fracture of the wood and of the adhesive. However, for the 1C-PUR adhesive, this is more challenging due to the transparency of the adhesive. To simplify the distinction (step 1 in Fig. 2), a chemical treatment of the samples using a reacting product was used (a solution of hydrochloric acid and phloroglucinol). This reagent colors the lignin in red allowing a better contrast between adhesive and wood, hence allowing distinguishing between adhesive and wood fracture. Approximatively one hour after applying the reagent, images of both fracture surfaces were taken with a digital single-lens reflex (DSLR) camera (24.2 megapixel APS-C 22.3×14.9 mm sensor) and a 100 mm macrolens. The final image resolution was one pixel ≈ 0.01 mm. Using the color difference (step 2 in Fig. 2), a color mask was applied using HSV color space to differentiate between the wood and adhesive fracture. Both images

were then binarized according to the color masks so that a black pixel (=0) corresponds to wood failure and a white pixel (=1) to adhesive failure. Both images were then superposed to obtain a map of the fracture surface using an OR filter so that if a pixel appears black (=0) it means that this pixel is black on both images, and hence indicates wood failure. This allows to distinguish between interface failure (one fracture surface fails in the wood and the opposite side in the adhesive) and wood failure. However, the distinction between wood and adhesive rupture based on color difference is not always exact, especially between zone boundaries. In addition, it is difficult to superpose and align both surfaces exactly. Both errors will overestimate the wood fracture percentage. To limit this error (step 3 in Fig. 2), only groups of interconnected black pixels which surfaces correspond to the different crack size estimation were considered in the calculation of the WFP. The main steps of the fractography method are summarized in Fig. 2.

Results and discussion

Estimation of the sensitivity of the acoustic emission measurements

Recent developments in the analysis of acoustic emission measurements (Brunner 2016) have shown that it is possible to establish an estimated correlation between crack area and the recorded linear AE signal amplitude (after amplification, measured in µV). A similar method is used here to estimate the damage size depending on the adhesive system. For each sample, the sum of the signal peak voltage is divided by the cracked surface. The cracked surface is estimated by multiplying the width of the specimen by the crack length increment measured during the test. This number is an estimation of the sensitivity and is given in ($\mu V/\mu m^2$). The crack length is measured on both lateral sides of the specimen, and the average value is taken for the calculation of the cracked surface. However, the exact crack tip position between these points is not known; therefore to consider a nonlinear crack tip position, upper and lower bounds are estimated by adding and, respectively, subtracting a half circle (with a diameter equal to the width of the specimen) to or from the cracked surface. Additionally, the surface roughness is considered by adding an arbitrary amount of 20% to the upper bound surface value. Using these estimations, lower and upper bounds are estimated for the sensitivity. Finally, the typical damage surface is computed by dividing the average amplitude of the signals (for one adhesive system) by the estimated sensitivity. Then, the square root of this surface is calculated to obtain the typical damage size (considering a quadratic or equivalent circular crack shape). The average sensitivity and expected crack size are given in Table 2 for the different adhesive systems.

The influence of the material damping (with a measured far-field damping value of 0.22 dB_{AE}/cm) on the estimated sensitivity was found to be less than 10% (estimated only from localized signals). Since attenuation was hence neglected, no AE signal amplitude correction as a function of distance was applied. In the next section, the UPR analysis was applied on the sample bonded using the HB 110 and PRF

Table 2 Estimated sensitivity and estimated crack size for a nonlinear crack tip propagation and for the different adhesive systems based on the AE signals amplitude—each value is given with upper and lower bounds

	Estimated sensitivity (μV/μm^2)			Estimated crack size (μm)		
	Mean	Upper bound	Lower bound	Mean	Upper bound	Lower bound
HB 110	7.5E−04	5.3E−04	9.4E−04	714	850	631
PRF	3.4E−03	2.4E−03	4.3E−03	363	433	321
VN 3158	2.3E−04	1.6E−04	2.9E−04	863	1028	763

adhesive, respectively. Due to the few signals ($n=2$) obtained for the samples glued with the adhesive VN 3158, no further analysis was considered in this case.

UPR on HB 110 adhesively bonded samples

The partition of all AE localized signals ($n=380$) obtained for the four different samples glued with the HB 110 adhesive are shown in Fig. 3. The best partition

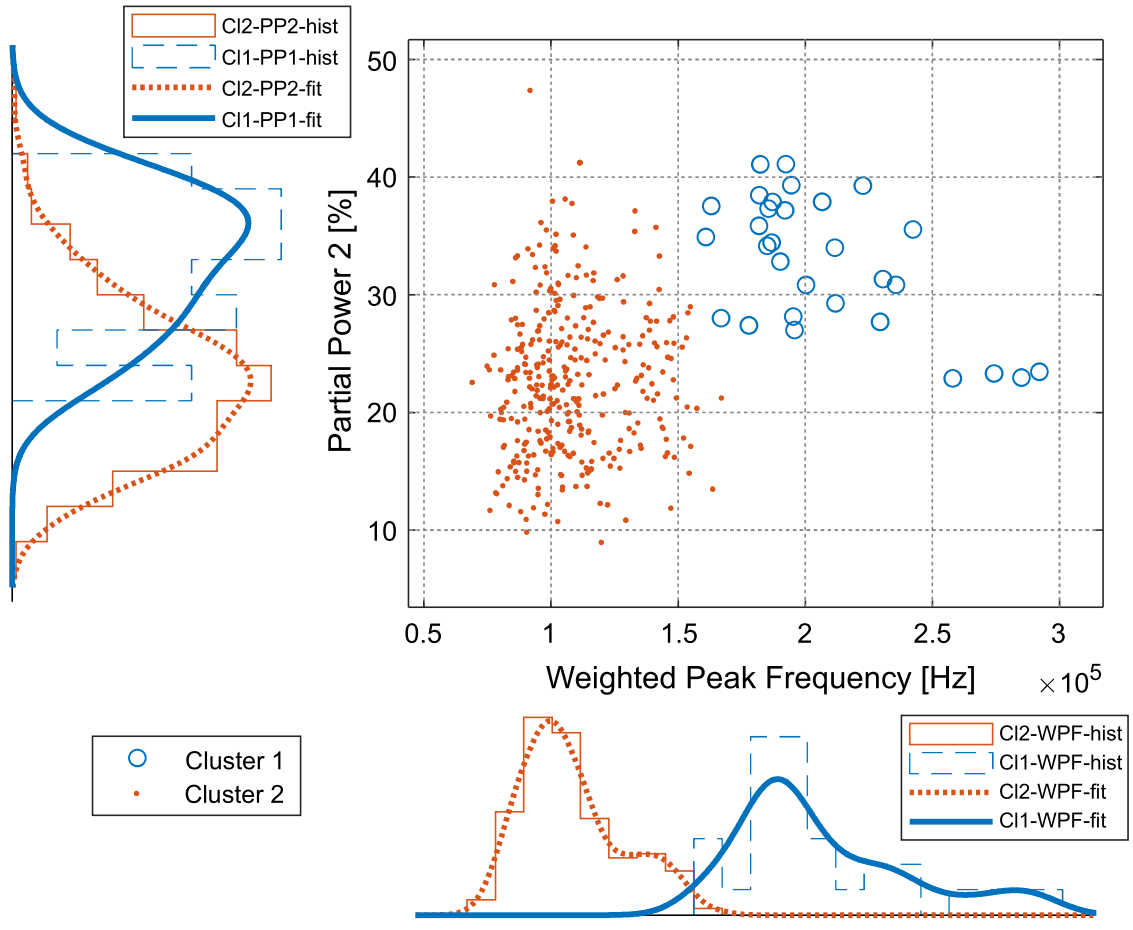

Fig. 3 Resulting partition of the AE signals in 2 clusters for the samples glued with the adhesive HB 110 according to the UPR method—Cl1: cluster 1, Cl2: cluster 2

is obtained with a direct use of the classifier algorithm with two clusters resulting in an uncertainty of classification (UoC) of 0.97 (Sause and Horn 2013), meaning that only 3% of the signals are potentially classified in the wrong cluster. In Fig. 3, marginal histograms are shown for both variables and both cluster data with a fitted line represent the data distribution. The number of bins was computed based on the sample standard deviation using Scott's rule. In further plots, only the fitted line was plotted to show the data distribution.

In Fig. 4, the relative timescale is compared with the estimated AE source position. The general tendency shown in Fig. 4 is that the position of the signal is increasing with the time duration and that it follows the approximate position of the crack tip. The signals from clusters 1 and 2 have a comparable temporal distribution.

On average, the energy of the signals from cluster 2 is higher than for cluster 1. However, no significant difference between the true energy distribution in clusters 1 and 2 was found (at a 5% significance level). In Figs. 3 and 4, all four HB 110 samples are shown in the same plot. However, the proportion for each sample was different as shown in Table 3.

The main difference between the clusters lies in their frequency characteristics, as the weighted peak frequency is clearly higher for cluster 1 compared to cluster 2. The physical meaning of different high-frequency proportions between clusters could be interpreted as originating from different microscopic sources,

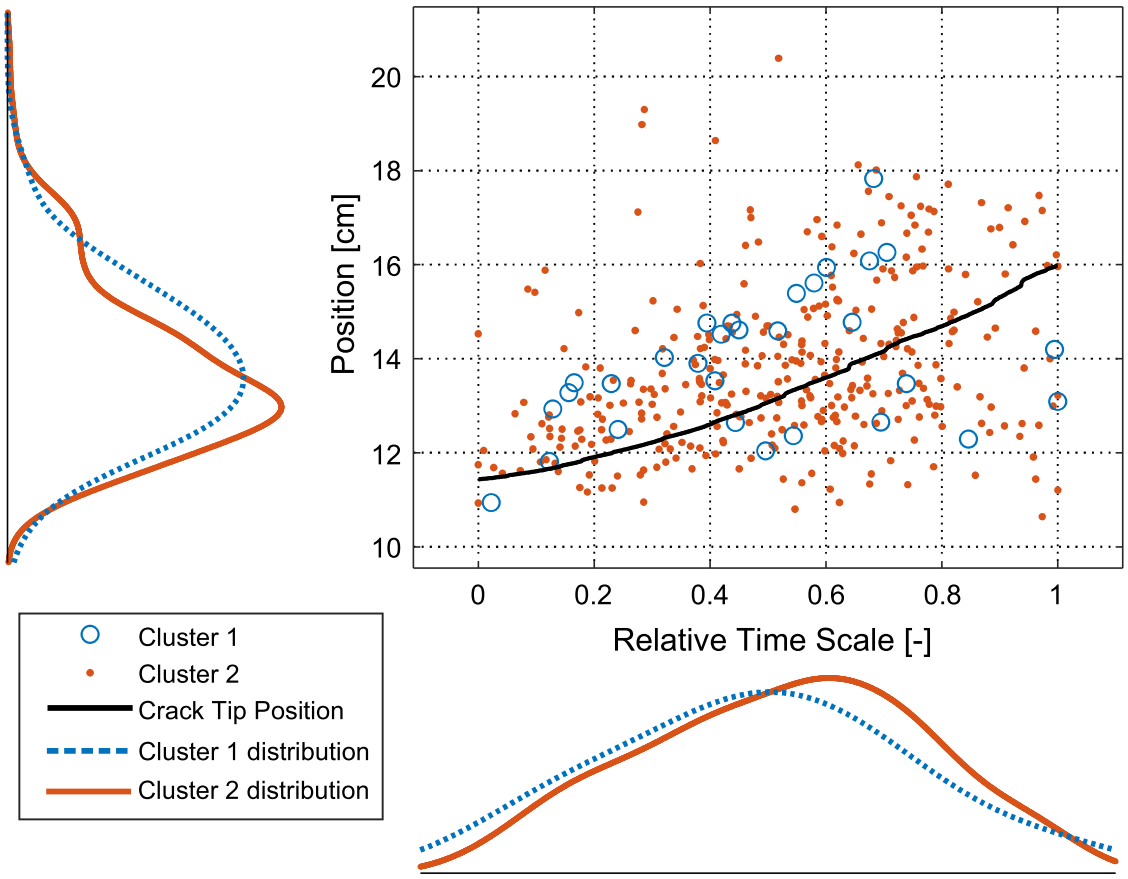

Fig. 4 Linear AE signal location, time and average crack tip position (calculated according to Clerc et al. 2019) for the four samples glued with the adhesive HB 110. Signals of both clusters follow the direction of the crack propagation

Table 3 Absolute and relative number of the signals for the adhesive HB 110 classified in clusters 1 and 2—the number of signals identified in cluster 1 is ranging from 0 to approximatively 10%

Sample	Signals from cluster 1	Signals from cluster 2
HB1a-2	4 (7%)	54 (93%)
HB3a-1	2 (3%)	60 (97%)
HB1a-1	7 (7%)	96 (93%)
HB3a-3	17 (11%)	138 (89%)

i.e., fracture mechanisms (Baensch et al. 2015a). To examine this hypothesis, an analysis of the fracture surface was conducted.

Prior to the analysis of the fracture surfaces, the estimated damage size was calculated (according to the above procedure) for each sample. These values were then used as lower, mean and upper range for estimating the crack size in the fractography analysis. The average wood fracture percentage is calculated by summing all the black pixel groups with a group size higher than the estimated lower crack size. Without lower limit, the estimated wood fracture percentage would be overestimated due to a high number of small pixel groups. Indeed, if all pixel groups are considered, the average group size is 0.03 mm^2. Given the size of these groups, they are probably due to the difficulty in superposing exactly two different images and to select the appropriate color filters to obtain the best distinction between wood and adhesive failure. Both phenomena will lead to a superposition of the same color area, interpreted as wood failure if black pixels are superposed.

The average wood fracture percentage obtained using the fractography analysis reveals a rough correlation between the number of signals associated with cluster 1 and the average WFP (Table 6). For example, it was noted that sample HB3a-1 had only 2 signals associated with cluster 2 (3%), whereas sample HB3a-3 had around 12% of its signals associated with cluster 2. The fractography analysis reveals that the average wood fracture percentage is below 0.1% for the HB3a-1 and around 7% for the HB3a-3.

The number of groups and their size is significantly higher for the HB3a-3 sample compared to the HB3a-1 sample (Fig. 5).

In comparison, both other samples (HB1a-1 and HB1a-2) show a relatively similar average wood fracture percentage (0.8% and 1.6%, respectively) and also a relatively similar percentage of signals associated with cluster 2 (7%). Considering the four samples, a correlation can be seen between the WFP and the number of signals associated with cluster 1. The higher weighted peak frequency observed in cluster 1 can be partly explained by the higher rigidity of the wood compared to the adhesive. Typically, cracks occurring in a brittle medium are expected to deliver a broad frequency spectrum. Defect-free beech as used here has a MOE of about 13 GPa, whereas adhesive stiffness is approximatively 1–4 GPa (with 1C-PUR ranging from 1 to 2 GPa and PRF from 3 to 4 GPa; Kläusler et al. 2013). Therefore, failure of the adhesive interface or cohesive failure is expected to result in AE signals with less broad frequency spectra. This translates into the different weighted peak frequencies found for the two clusters.

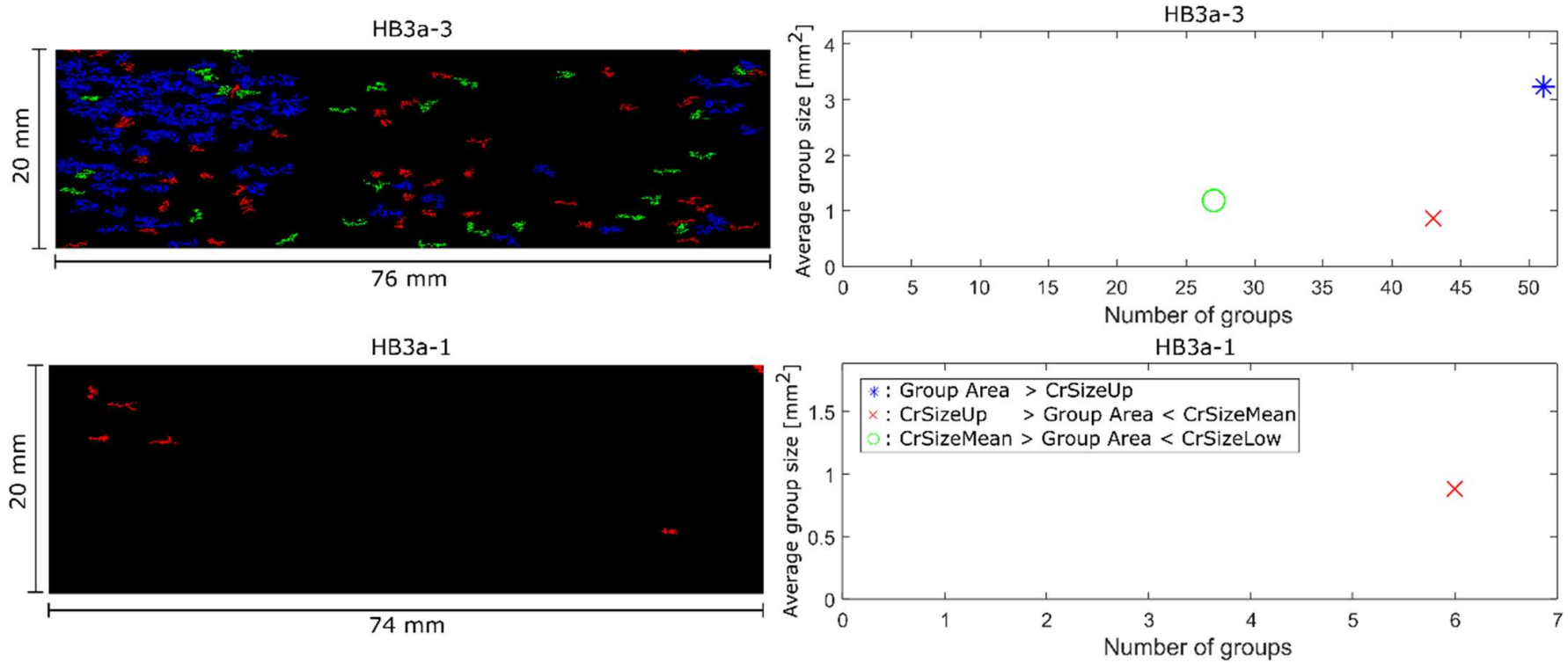

Fig. 5 Fractography results for the sample HB3a-3 (top) and HB3a-1 (bottom) showing the different groups of pixels associated with wood fracture according to the estimated crack size

PRF adhesive

The partition of all localized AE signals ($n = 1927$) obtained for the four different samples glued with the PRF adhesive is shown in Fig. 6. The best partition is obtained with a direct use of the classifier algorithm with two clusters with an UoC of 0.91.

The number of signals obtained from the PRF samples is much higher than for the HB 110 samples. This could be an indication of a larger effective fracture surface due to higher roughness or due to a smaller crack increment per AE signal due to the more brittle PRF adhesive. The average energy per hit for cluster 1 of the PRF (Table 7) is very similar to cluster 1 of the HB 110 adhesive (Table 4). On average, a higher number of signals is classified in cluster 1 (Table 5) in comparison with the HB 110 adhesive, the majority being still classified into cluster 2 (Table 6). On average, a higher weighted peak frequency is obtained for cluster 1 than for cluster 2 (Table 7). In comparison with the adhesive HB 110, the average weighted peak frequency from clusters 1 and 2 is higher for the PRF adhesive (approx. 20%) (Table 7).

Contrary to the samples glued with the adhesive HB 110, the number of signals associated with cluster 1 tends to increase nonlinearly with the test duration (Fig. 7). In comparison, the number of signals from cluster 2 increases gradually until the

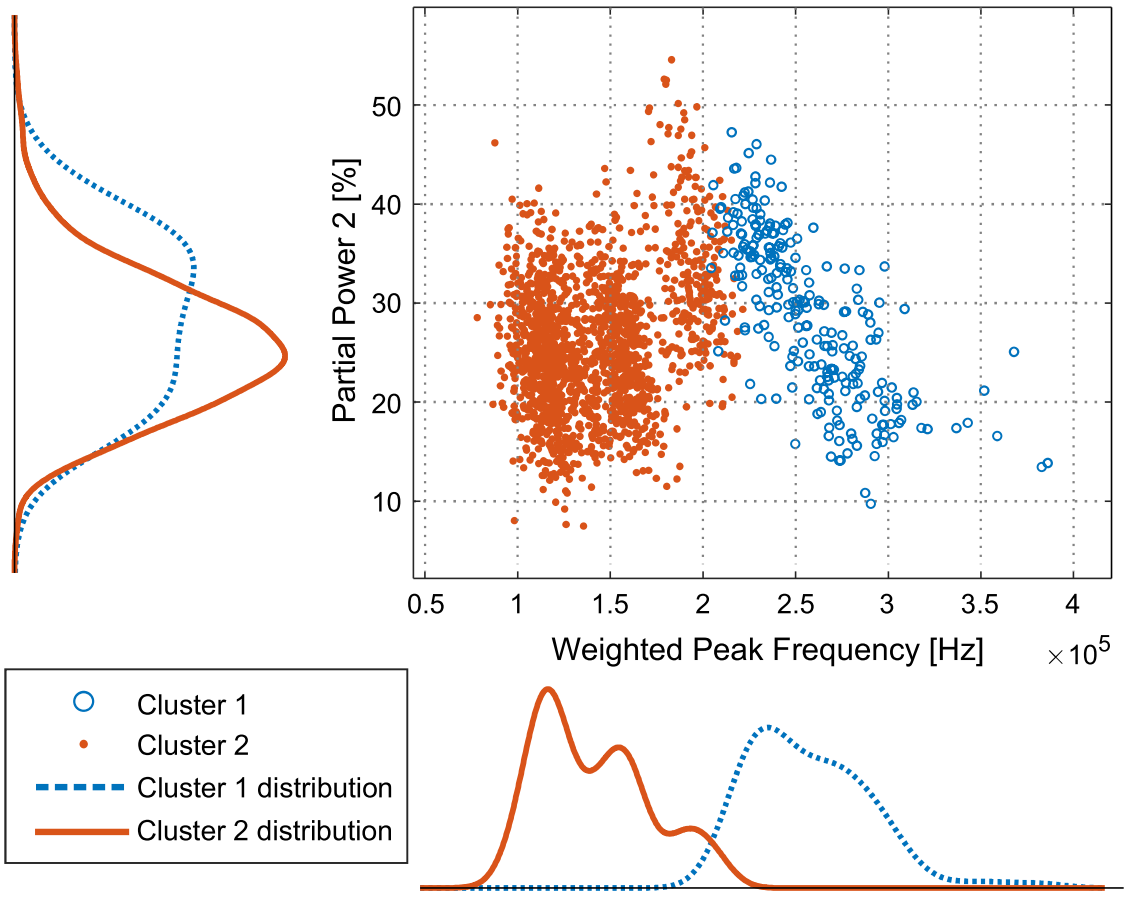

Fig. 6 Resulting partition of the AE signals in 2 clusters for the samples glued with the adhesive PRF according to the UPR method

Table 4 Main differences between the signals associated with cluster 1 and cluster 2

	Cluster 1	Cluster 2
Number (quota)	30 (8%)	348 (92%)
Energy sum (quota)	2.5860e−15 (1%)	4.9583e−13 (99%)
Energy per hit (J) (median)	1.9831e−17	5.5038e−17
Partial power 2 (%)	32.7	22.8
Weighted peak frequency (kHz)	207.3	108.3

Table 5 Absolute and relative classification of the signals in cluster 1 and cluster 2 for the PRF samples—the number of signals identified in cluster 1 ranges from 10% to approximatively 20%

Sample	Signals from cluster 1	Signals from cluster 2
PRF3B-1	93 (14%)	590 (86%)
PRF2B-1	44 (11%)	351 (89%)
PRF2B-2	44 (18%)	205 (82%)
PRF2B-5	62 (11%)	494 (89%)

Table 6 Average wood fracture percentage (WFP) obtained from the cluster analysis and corresponding estimated crack size, mean and upper and lower bounds for the samples glued with the adhesive HB 110

Sample	Average WFP (%)	Crack size mean value (μm)	Crack size up. Bound value (μm)	Crack size low. Bound value (μm)
HB1a-2	1.6	663	788	590
HB3a-1	<0.1	721	859	637
HB1a-1	0.8	510	603	457
HB3a-3	7	656	775	568

Table 7 Main differences between the signals associated with cluster 1 and cluster 2 for the PRF samples

	Cluster 1	Cluster 2
Size (quota)	243 (13%)	1640 (87%)
Energy sum (J) (quota)	3.81e−14	4.96e−13
Energy per hit (J) (median)	1.9453e−17	2.5276e−17
Partial power 2 (%)	28.6	26.0
Weighted peak frequency (kHz)	257.6	141.3

end of the test, but the number of signals from cluster 1 increases significantly only after 50% of the relative timescale.

Using the fractography method as described above, it is possible to distinguish between wood fracture and adhesive failure (using the natural contrast between the wood and the dark brown PRF adhesive). Summing the number of pixels associated with wood failure over the cracked surfaces reveals that the crack is generally starting as an interface failure but evolves gradually into wood failure as shown in Fig. 8.

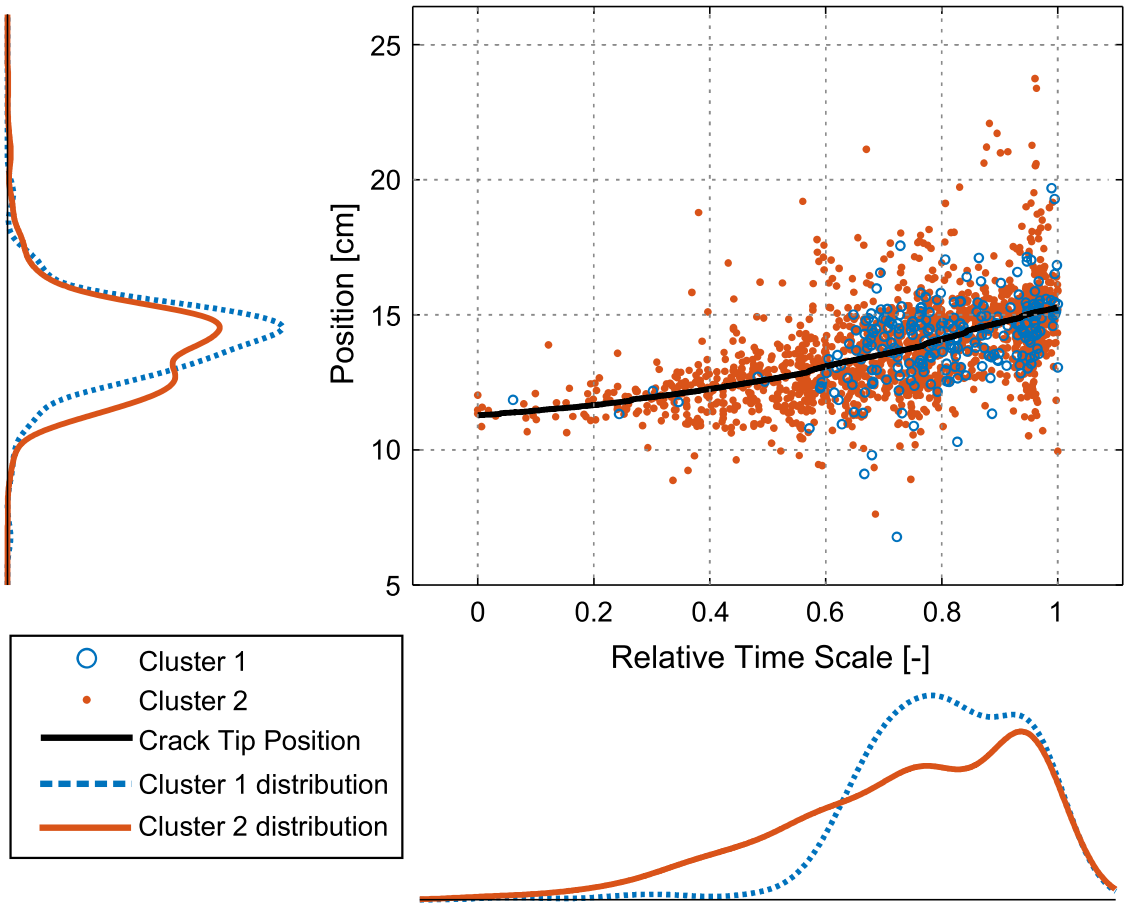

Fig. 7 AE signal location, time and average crack tip position for the four samples glued with the adhesive PRF. Signals of both clusters follow the direction of the crack propagation

Influence of the adhesive system on the cluster features

It has been shown that for both adhesive systems, it was possible to roughly correlate the signals from the lower-frequency cluster 1 with wood failure. It was also noted that for the samples glued with the PRF adhesive, a higher number of signals were recorded than for the HB 110 adhesive. Furthermore, the estimated average crack increment is smaller for the PRF system than for the HB 110. One further difference is that for the PRF adhesive, the crack is growing into the wood and propagates into the wood for most of the samples, whereas for the HB 110 samples, the crack propagates at the interface essentially due to an adhesive failure. Only a small fraction of the fracture surface corresponds to wood failure. This could indicate that the propagation medium of the HB 110 is more homogenous and fewer obstacles have to be overcome during the crack growth, whereas for the PRF samples, the crack has to propagate through the highly fibrous environment of the wood. This hypothesis seems to be confirmed by the very low number of signals obtained from the VN adhesive, which is even more homogenous (due to the absence of polyamide fibers in the adhesive matrix but also due to the more ductile behavior of the adhesive). For the PRF samples, even though the number of signals associated with cluster 1 tends to correlate with the wood fracture percentage, the majority of the signals are still associated with cluster

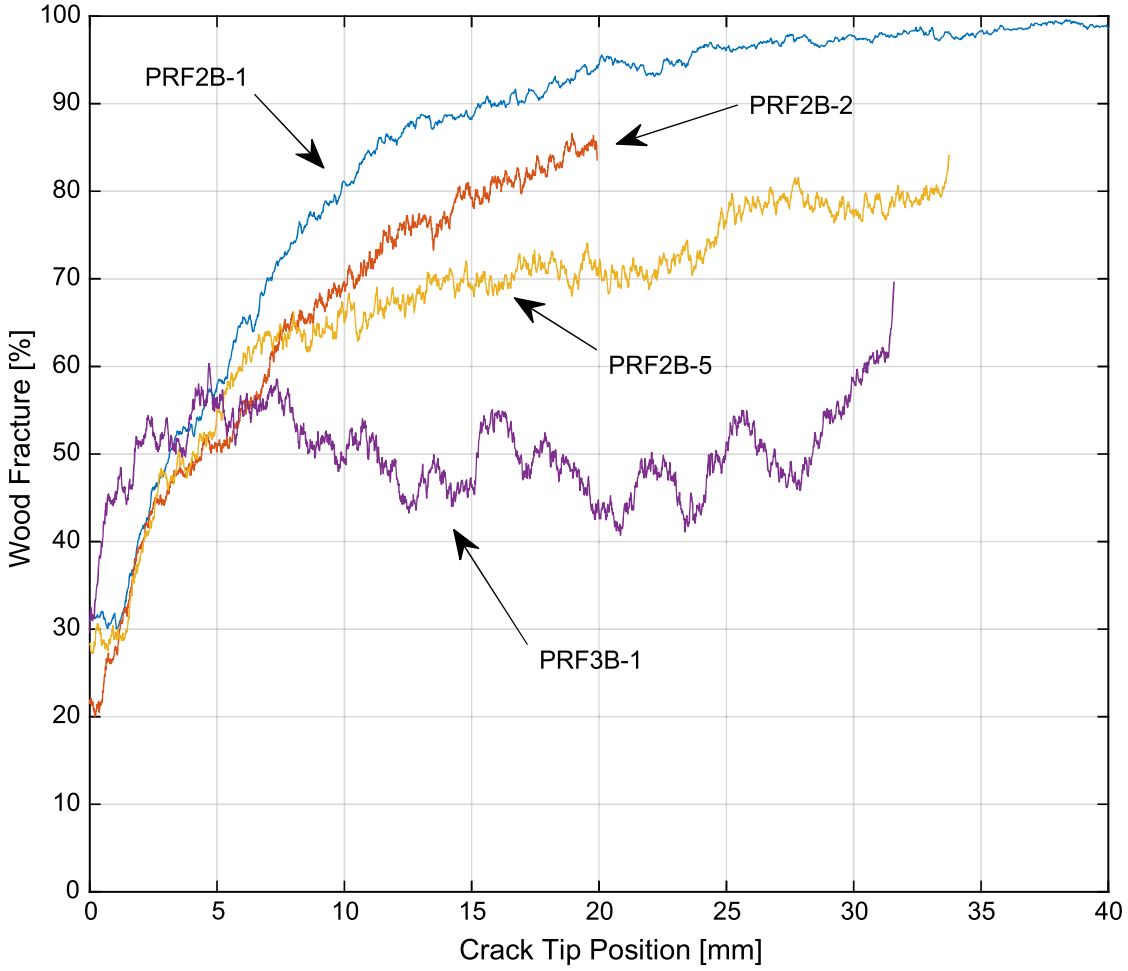

Fig. 8 Increase in the wood fracture percentage with increasing crack length for the samples glued with the PRF adhesive

2 even when the crack is mostly propagating into the wood. The exact reason for this is not yet completely understood, but it may be that since beech stiffness perpendicular to the grain is around 1 GPa, if the crack follows a path under an angle with the grain, the stiffness may well be in the same range as that of PRF. It may also be that this difference is due to different failure mechanisms occurring in plain wood. As shown in Fig. 9, the fracture surface is a complex patchwork of different wood anatomical features. It can be expected that failures of different anatomical features have different acoustic patterns and that some failure mechanisms have a similar acoustic pattern to interface failure, which would lead to classification in the same clusters. In addition, as shown in Fig. 6, it is possible that more clusters exist than those investigated in this study. However, partitions with more than two clusters results in a lower UoC, meaning that potentially more signals would be classified into the wrong clusters. For this reason, this was not further considered.

It seems therefore that crack propagation into the wood is advantageous as the crack has a higher number of obstacles (or obstacles that yield higher energy dissipation) to overcome in order to propagate, hence generating AE signals. This

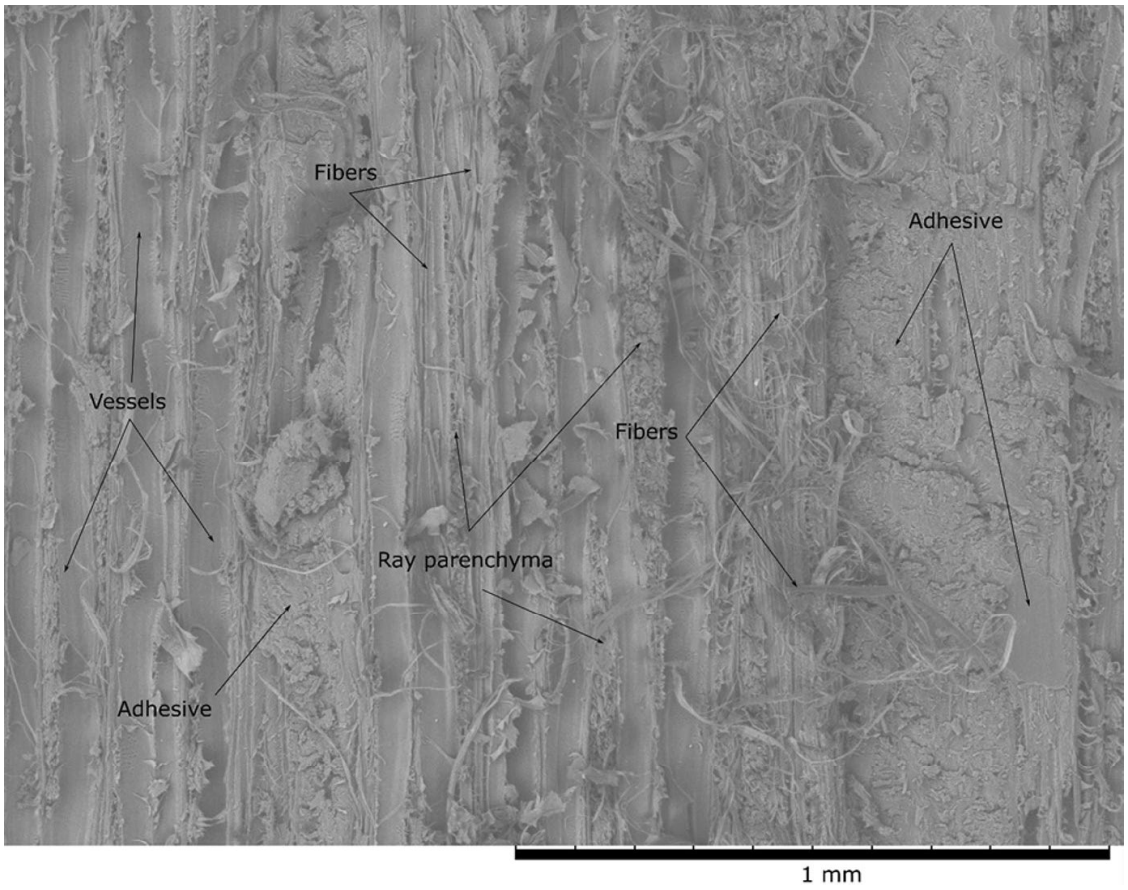

Fig. 9 SEM image of the fracture surface of one PRF sample showing the different anatomical features failing during the crack propagation—each feature with a possible distinct AE pattern

hypothesis corresponds to the results obtained by Clerc et al. (2019), where in quasi-static 4-ENF Mode II tests PRF samples had typically a slower crack propagation compared to the HB 110 adhesive, which itself had a slower crack propagation than the VN 3158 adhesive.

For further adhesive development, an optimal adhesive system would need to have a low MOE for absorbing the damages, but a high cohesive and adhesive strength so that the easiest growth path for the crack is in the wood. It is, however, questionable whether it is possible to obtain an adhesive with a low MOE and a high cohesive/adhesive strength as generally a highly cross-linked polymer has a high MOE and a high cohesive/adhesive strength due to the greater number of links available for bonding with the adherent.

During shear loading, the main causes of rupture in the wood are probably associated with interwall (middle lamella) cracks (Fig. 9). The average weighted peak frequency of cluster 1 of both adhesives is around 200–250 kHz, which corresponds approximatively to cluster A presented by Baensch et al. (2015a). Vergeynst et al. (2014) have shown, by using FEM modeling of signal propagation in wood, that the brittle rupture phenomenon will generate signals with a higher WFP, whereas the ductile rupture phenomenon will result in signals with a lower WFP. It should, however, be added that, even though the speed of the mechanism leads to a shorter or longer rise time of the source (voltage/load build-up), this will influence the rise

time of the signals, but also the frequency spectrum. The higher-frequency components of the signals will be more attenuated in the material than low-frequency components. Therefore, this will also depend on the source–sensor distance and its material properties. With an average WFP of ~ 600 kHz, the signals of cluster B found by Baensch et al. (2015a) have a much higher WFP than the signals obtained in the present study. This could be due to the more brittle rupture of the wood obtained under tension loading and/or to different rupture phenomena occurring between softwood (spruce in the case of Baensch et al. 2015b) and hardwood in the present study. Cluster B in Baensch et al. (2015b) was associated with the transversal cell wall cracks in the RT plane, a type of rupture which was not observed on the tested samples. As shown in Fig. 9, the main type of wood rupture was interwall/cell wall cracks in the LT/LR plane. This confirms the results obtained by Ando et al. (2006), where under shear loading, mainly interwall (middle lamella) failure of wood was observed.

One further point to discuss is that the present analysis was specifically conducted on samples tested under quasi-static loading. AE measurements were also taken on samples tested under cyclic loading but were not analyzed as the signal/noise ratio was too high for dedicated AE analysis. Further, as noted by Clerc et al. (2019), cyclic loaded PRF samples had a lower wood fracture percentage as typically observed under quasi-static loading. However, the average wood fracture of these samples remains higher than for 1C-PUR-bonded samples. It can therefore be assumed that the presented hypotheses are still valid (but probably to a lesser extent) in case of cyclic fracture loading. Nevertheless, this should be confirmed with additional tests.

Conclusion

For both adhesive systems, PUR and PRF, it was possible to show that the AE signals associated with cluster 1 correspond to wood fracture. The proposed method of associating fractography with acoustic emission allows estimating even a very small percentage of wood failure through a higher resolution of the cracked surfaces. The following points can be summarized:

- Two types of clusters could be identified for two different types of adhesive; these clusters seem to correspond to different failure mechanisms in the bond line, cluster 2 being associated with crack propagation in the interface and cluster 1 being associated with crack propagation in the wood layer near the interface.
- By using fractography, it was shown that the size and number of pixel groups associated with wood failure reflect the number of signals corresponding to cluster 1 for the adhesive HB 110.
- It was shown for the adhesive PRF that the number of signals associated with cluster 1 is increasing with the test duration. Comparing the fracture surface, it was shown that the crack is starting from an adhesive failure type and propagates into the wood, hence reflecting the signal classification into cluster 1.

The presented results suggest that the addition of short fibers (< 1 mm) in an adhesive helps slowing down the crack propagation. The addition of fibers in the adhesive may, however, be limited for practical reasons (viscosity too high, agglomeration of fibers and difficulty in obtaining a uniform application). In addition, it seems that the wood structure is more efficient in slowing the crack than the modified 1C-PUR adhesive. Further research on adhesive development should focus on obtaining a transition of the fracture surface away from the interface into the wood to improve the crack propagation resistance of relatively ductile wood adhesives.

Acknowledgements The authors thank Dr. Sébastien Josset (Henkel AG) for providing 1C-PUR adhesives as well as the Swiss Innovation Agency (Innosuisse) for the financial support (Project No. 18958.1).

Compliance with ethical standards

Conflict of interest On behalf of all authors, the corresponding author states that there is no conflict of interest.

References

Aicher S, Höfflin L, Dill-Langer G (2001) Damage evolution and acoustic emission of wood at tension perpendicular to fiber. Holz Roh Werkst 59:104–116. https://doi.org/10.1007/s001070050482

Ando K, Hirashima Y, Sugihara M, Hirao S, Sasaki Y (2006) Microscopic processes of shearing fracture of old wood, examined using the acoustic emission technique. J Wood Sci 52:483–489. https://doi.org/10.1007/s10086-005-0795-7

Baensch F, Sause MGR, Brunner AJ, Niemz P (2015a) Damage evolution in wood-pattern recognition based on acoustic emission (AE) frequency spectra. Holzforschung. https://doi.org/10.1515/hf-2014-0072

Baensch F, Zauner M, Sanabria SJ, Sause MGR, Pinzer BR, Brunner AJ, Stampanoni M, Niemz P (2015b) Damage evolution in wood: synchrotron radiation micro-computed tomography (SRμCT) as a complementary tool for interpreting acoustic emission (AE) behavior. Holzforschung 69:1015–1025. https://doi.org/10.1515/hf-2014-0152

Brunner AJ (2016) Correlation between acoustic emission signals and delaminations in carbon fiber-reinforced polymer-matrix composites: a new look at mode I fracture test data. In: 32nd European conference on acoustic emission testing Czech society for nondestructive testing, Prague

Brunner AJ, Baensch F, Sause MGR, Zauner M, Niemz P (2015) Schallemissionsanalyse und Synchrotron-basierte Mikrotomografie an verklebten Miniatur-Zugprüfkörpern aus Fichtenholz. DGZfP 20. Kolloquium Schallemission, Garmisch-Partenkirchen [Acoustic emission analysis and synchroton-based microtomography on glued shear strength samples from spruce solid wood]

Chen G, Luo H, Wu S, Guan J, Luo J, Zhao T (2018) Flexural deformation and fracture behaviors of bamboo with gradient hierarchical fibrous structure and water content. Compos Sci Technol 157:126–133. https://doi.org/10.1016/j.compscitech.2018.01.034

Clerc G, Brunner AJ, Josset S, Niemz P, Pichelin F, van de Kuilen JWG (2019) Adhesive wood joints under quasi-static and cyclic fatigue fracture Mode II loads. Int J Fatigue 123:40–52. https://doi.org/10.1016/j.ijfatigue.2019.02.008

Diakhate M, Bastidas-Arteaga E, Moutou Pitti R, Schoefs F (2017) Cluster analysis of acoustic emission activity within wood material: towards a real-time monitoring of crack tip propagation. Eng Fract Mech 180:254–267. https://doi.org/10.1016/j.engfracmech.2017.06.006

Hass P, Kläusler O, Schlegel S, Niemz P (2014) Effects of mechanical and chemical surface preparation on adhesively bonded wooden joints. Int J Adhes Adhes 51:95–102. https://doi.org/10.1016/j.ijadhadh.2014.02.014

Jakieła S, Bratasz Ł, Kozłowski R (2008) Acoustic emission for tracing fracture intensity in lime wood due to climatic variations. Wood Sci Technol 42:269–279. https://doi.org/10.1007/s00226-007-0156-3

Kläusler O, Clauß S, Lübke L, Trachsel J, Niemz P (2013) Influence of moisture on stress–strain behaviour of adhesives used for structural bonding of wood. Int J Adhes Adhes 44:57–65. https://doi.org/10.1016/j.ijadhadh.2013.01.015

Kläusler O, Hass P, Amen C, Schlegel S, Niemz P (2014) Improvement of tensile shear strength and wood failure percentage of 1C PUR bonded wooden joints at wet stage by means of DMF priming. Eur J Wood Prod 72:343–354. https://doi.org/10.1007/s00107-014-0786-8

Lehringer C, Gabriel J (2014) Review of recent research activities on one-component PUR-adhesives for engineered wood products. In: Aicher S, Reinhardt HW, Garrecht H (eds) Materials and joints in timber structures. RILEM Bookseries, vol 9. Springer, Dordrecht

Najafi SK, Sharifnia H, Najafabadi MA, Landis E (2017) Acoustic emission characterization of failure mechanisms in oriented strand board using wavelet based and unsupervised clustering methods. Wood Sci Technol 51:1433–1446. https://doi.org/10.1007/s00226-017-0946-1

Reiterer A, Stanzl-Tschegg SE, Tschegg EK (2000) Mode I fracture and acoustic emission of softwood and hardwood. Wood Sci Technol 34:417–430. https://doi.org/10.1007/s002260000056

Sause MGR, Horn S (2013) Quantification of the uncertainty of pattern recognition approaches applied to acoustic emission signals. J Nondestruct Eval 32:242–255. https://doi.org/10.1007/s10921-013-0177-9

Sause MGR, Gribov A, Unwin AR, Horn S (2012a) Pattern recognition approach to identify natural clusters of acoustic emission signals. Pattern Recognit Lett 33:17–23. https://doi.org/10.1016/j.patrec.2011.09.018

Sause MGR, Müller T, Horoschenkoff A, Horn S (2012b) Quantification of failure mechanisms in mode-I loading of fiber reinforced plastics utilizing acoustic emission analysis. Compos Sci Technol 72:167–174. https://doi.org/10.1016/j.compscitech.2011.10.013

Vergeynst LL, Sause MGR, Ritschel F, Brunner AJ, Niemz P, Steppe K (2014) Finite element modelling used to support wood failure identification based on acoustic emission signals. In: Franke S, Franke B, Widmann R (eds) COST timber bridge conference. Bern University of Applied Sciences, Bern, pp 141–146